JGR Solid Earth

RESEARCH ARTICLE
10.1029/2024JB029792

Low-Degree Spherical Harmonic Coefficients for GRACE/GRACE-FO Gravity Field Models From the Fingerprint Approach

Changlin Mei[1,2,3], **Yu Sun**[1,2,3], **and Yang Li**[4,5]

[1]Key Lab of Spatial Data Mining and Information Sharing, Ministry of Education, Fuzhou University, Fujian, China, [2]National Engineering Research Center of Geospatial Information Technology, Fuzhou University, Fujian, China, [3]National & Local Joint Engineering Research Center of Satellite Geospatial Information Technology, Fuzhou University, Fujian, China, [4]State Key Laboratory of Geodesy and Earth's Dynamics, Innovation Academy for Precision Measurement Science and Technology, Chinese Academy of Sciences, Wuhan, China, [5]University of Chinese Academy of Sciences, Beijing, China

Abstract Low-degree coefficients of time-variable gravity field models from Gravity Recovery and Climate Experiment (GRACE) and GRACE-Follow On (GRACE-FO) capture large-scale mass changes within the Earth system. However, some of these coefficients are either missing (e.g., degree-1 coefficients) or poorly determined (e.g., C_{20}). Such a situation is exacerbated particularly over the GRACE-FO period when one of the accelerometers carries elevated noise. In this study, we present a framework for estimating low-degree coefficients using the fingerprint approach. Our results demonstrate that this method can reliably estimate multiple coefficients simultaneously, producing degree-1, C_{20}, and C_{30} estimates that are comparable to the currently recommended solutions, both in direct comparisons and in the context of estimating mass changes over the Antarctic Ice Sheet. This framework not only provides an alternative approach for determining low-degree coefficients currently identified as problematic in GRACE/GRACE-FO gravity field models, but also shows potential for addressing other degraded low-degree coefficients that may emerge during future GRACE-FO operations.

Plain Language Summary Time-variable gravity field models from GRACE and GRACE-Follow On (GRACE-FO) are invaluable for directly measuring mass changes in the Earth system. However, during the GRACE-FO period, one of the accelerometers experienced higher noise levels, and the mission cannot fully exploit the information provided by two accelerometers. This limitation affected the accuracy of certain key measurements, particularly low-degree coefficients, which are essential for understanding large-scale mass redistribution. In this study, we present a method to estimate these problematic coefficients simultaneously. Our results, which include estimates related to geocenter motion and the Earth's changing shape (dynamic oblateness), are consistent with the most advanced existing solutions. This framework also holds potential for estimating other degraded coefficients that may emerge during the GRACE-FO mission in the future.

Key Points:

- A framework for estimating multiple low-degree coefficients using the fingerprint approach is presented and explained
- The fingerprint approach effectively enables the simultaneous estimation of multiple low-degree coefficients
- The resulting degree-1, C_{20}, and C_{30} coefficients are comparable to the recommended solutions, both in direct comparisons and in the context of estimating mass changes over Antarctica

Supporting Information:

Supporting Information may be found in the online version of this article.

Correspondence to:

Y. Sun,
jade.yusun@outlook.com

Citation:

Mei, C., Sun, Y., & Li, Y. (2025). Low-degree spherical harmonic coefficients for GRACE/GRACE-FO gravity field models from the fingerprint approach. *Journal of Geophysical Research: Solid Earth*, *130*, e2024JB029792. https://doi.org/10.1029/2024JB029792

Received 25 JUN 2024
Accepted 8 JUL 2025

Author Contributions:

Conceptualization: Changlin Mei, Yu Sun, Yang Li
Data curation: Changlin Mei, Yang Li
Formal analysis: Changlin Mei, Yu Sun
Funding acquisition: Yu Sun
Investigation: Changlin Mei, Yu Sun, Yang Li
Methodology: Changlin Mei, Yu Sun, Yang Li
Resources: Changlin Mei
Software: Changlin Mei, Yu Sun, Yang Li
Supervision: Yu Sun
Validation: Changlin Mei, Yu Sun, Yang Li
Visualization: Changlin Mei, Yang Li
Writing – original draft: Changlin Mei, Yu Sun
Writing – review & editing: Changlin Mei, Yu Sun, Yang Li

1. Introduction

The Gravity Recovery and Climate Experiment (GRACE) and its successor, GRACE Follow-On (GRACE-FO), have been providing gravity field models on a monthly basis for over two decades (Landerer et al., 2020; Tapley et al., 2004). These unique measurements are directly related to mass changes at the Earth's surface after the removal of signals originated from the interior of the solid Earth, including those caused by the Glacial Isostatic Adjustment (GIA) (Caron et al., 2018; Peltier et al., 2018) and mega-thrust earthquakes (Han et al., 2013). Surface mass variations, primarily driven by the atmosphere, oceans, glaciers, and terrestrial water within the fluid envelope of the Earth system, are recognized as critical data records to better understand climate change and climate variability (National Academies of Sciences, Engineering, and Medicine, 2018; Tapley et al., 2019). GRACE and GRACE-FO gravity field models are typically provided as spherical harmonic coefficients, but these products require post-processing techniques, such as decorrelation filtering and smoothing (Klees et al., 2008; Kusche et al., 2009; Swenson & Wahr, 2006), to remove the prominent north-south stripes. For the convenience of application-oriented users, several data centers have released mascon solutions provided directly in gridded equivalent water height. These products do not require additional filtering techniques owing to the regularization strategies applied at the inversion stage. However, both products still face challenges related to certain low-degree

coefficients, particularly degree-1, C_{20}, and C_{30}, which are critical for capturing large-scale mass changes in the Earth system. Degree-1 coefficients are related to the geocenter motions, defined as the motion of the center-of-figure of the solid Earth (CF) relative to the center-of-mass of the entire Earth system (CM). C_{20} coefficients, also known as J_2 ($J_2 = -\sqrt{5}C_{20}$), represent changes in the Earth's dynamic oblateness. C_{30} and other low-degree zonal coefficients are critical for estimating polar mass changes.

It is difficult to improve the quality of the aforementioned low-degree coefficients. Geocenter motions cannot be determined solely from the inter-satellite range/range-rate data of the GRACE/GRACE-FO mission, as these coefficients are zeros by definition in the CM reference frame. To estimate these coefficients in the CF reference frame, additional data sets are needed, such as those from Satellite Laser Ranging (SLR) (Gałdyn & Sośnica, 2024), on-board Global Positioning System (GPS) (Kang et al., 2019), and oceanic degree-1 coefficients from modeled estimates of ocean bottom pressure (OBP) model (Swenson et al., 2008). The C_{20} coefficients are poorly determined due to unexpected non-geophysical signals from the accelerometers (Cheng & Ries, 2017) as well as tidal-aliasing errors (Chen & Wilson, 2008). The intentional powering off of an accelerometer toward the ending stage of the GRACE mission and the elevated noise in the GFO-2 accelerometer of the GRACE-FO mission (degraded periods, after August 2016) exacerbated the situation. During these periods, non-gravitational forces (e.g., atmospheric drag, solar radiation pressure) could no longer be directly and accurately measured by both satellites. To compensate for the missing data, an approach known as accelerometer transplant is implemented. This method synthetically reconstructs GFO-2 accelerometer data using measurements from the functioning GFO-1 accelerometer. It incorporates time shifts and attitude corrections to account for the relative motion and orientation between the two spacecraft, along with model-based adjustments for thruster firings to better capture residual accelerations (Bandikova et al., 2019; Behzadpour et al., 2021). Although this approach allows continued gravity field recovery, it remains imperfect due to satellite-specific environmental differences and modeling limitations, resulting in elevated noise and reduced accuracy-particularly affecting the low-degree zonal coefficients (Behzadpour et al., 2021). In fact, not only C_{20} coefficients but also C_{30} coefficients are of worse quality compared to those during the period when the two accelerometers were fully functional (nominal period, from April 2002 to July 2016). Due to the ongoing degradation of low-degree coefficients, several updated GRACE-FO gravity field solutions have been released since Release 06 (RL06). RL06.1 adopts a new set of the Level-1B accelerometer transplant data, while RL06.2, released only currently by CSR, increases the available GPS data volume and updates the weighting between K-Band Ranging and GPS data after June 2020. These improvements result in better low-degree coefficient estimates in RL06.2 after 2022. Recently, all three data centers updated to RL06.3, which differs from RL06.1 only in the Level-1B accelerometer transplant data used for the GFO-2 satellite. This update applies only to data from January 2023 onward during wide-deadband operations; data from June 2018 to December 2022 remain identical between RL06.1 and RL06.3. However, despite these sophisticated processing techniques, replacing the C_{20} and C_{30} coefficients with data based on SLR is still recommended (Cheng & Ries, 2023; Loomis et al., 2020). This prompted us to develop methods to refine these problematic coefficients.

Currently, several methods have the potential to simultaneously estimate multiple coefficients. SLR processing can provide low-degree coefficients up to degree 10 (Sośnica et al., 2014), including C_{20} and C_{30} coefficients that are currently recommended as replacement for their GRACE/GRACE-FO counterparts (Cheng & Ries, 2023; Loomis et al., 2020). Although degree-1 coefficients can also be derived from SLR, they are not yet routinely used to complete GRACE/GRACE-FO gravity field models. Moreover, seasonal artifacts in SLR-based solutions due to unmodeled tropospheric delays, station-specific range biases, and surface mass loading effects may lead to unrealistic mass change estimates (Sun et al., 2017). Global GPS inversion uses the GPS-sensed low-degree surface deformation to invert for low-degree coefficients (Blewitt et al., 2001; Kusche & Schrama, 2005; Razeghi et al., 2019; Wu et al., 2006). However, extracting load-induced signals in GPS data and overcoming network effects due to uneven GPS station distribution remain challenging (Zajdel et al., 2019). Additionally, the resulting solution often lacks linear trends because they are removed to exclude solid Earth signals. An alternative solution for estimating geocenter motion was derived by Swenson et al. (2008) by combining the GRACE data with output from an OBP model. Such a method essentially relies on the OBP model to provide the mass change values in the CF frame. These differences, when compared to those based on GRACE in the CM frame, can be used to estimate degree-1 coefficients. The GRACE-OBP method is further developed to jointly estimate C_{20}, C_{21}, S_{21}, and C_{30} coefficients (Seo et al., 2021; Sun et al., 2023; Sun, Ditmar, & Riva, 2016; Sutterley & Velicogna, 2019). However, OBP inputs are not accompanied by uncertainty estimates. Evaluation of their

low-degree coefficients is needed to understand their impact on the final results. Additionally, uncertainties in the input data will be magnified according to the error propagation law. Amplification factors vary for different coefficients and grow rapidly with an increase in the number of co-estimated coefficients (Sun, Riva, & Ditmar, 2016).

The fingerprint approach (see Section 2.1) was proposed by Rietbroek et al. (2012, 2016). In their work, the authors estimated degree-1 coefficients to address sea level contributions by combining GRACE and altimetry data. Sun et al. (2019) estimated C_{20} coefficients using only GRACE data, agreeing with results from SLR and GRACE-OBP. This method has the potential to estimate multiple coefficients simultaneously. In this study, we apply the fingerprint approach to estimate the degree-1, C_{20}, and C_{30} coefficients and evaluate their impact on estimating mass changes over the Antarctic Ice Sheet (AIS).

2. Methodology and Input Data

2.1. Methodology

Fingerprints are distinct spatial patterns of gravity field variations or relative sea level changes linked to mass changes over the continents. It is predicted by theory (Farrell, 1972) and recently observed, for instance, in oceanic regions near Greenland (Coulson et al., 2022). The fundamental premise of the fingerprint method posits that global surface mass changes can be sufficiently represented by a limited number of partitioned mass change blocks/modes. The spatial distributions of mass change within these blocks/modes must be known in advance; otherwise, the blocks can be subdivided into smaller ones until the criterion is satisfied (Rietbroek et al., 2016). Once determined, the sea level fingerprint for each block/mode can be calculated by solving the sea level equation (Tamisiea et al., 2010). The resulting fingerprints describe the redistribution of surface mass, a process governed by changes in relative sea level, which is invariant across reference frames. Because this redistribution induces motion between the CM and the CF, each fingerprint inherently includes a degree-1 component. In contrast, the degree-0 term is always set to zero, reflecting the assumption of mass conservation within the Earth system. These fingerprints effectively serve as basis functions. Given a set of fingerprints, the observed gravity fields can be forward-modeled as follows:

$$\underset{m\times k}{\mathbf{b}} = \underset{m\times n}{\mathbf{A}}\ \underset{n\times k}{\mathbf{X}}, \tag{1}$$

where $\mathbf{A}$ denotes the matrix containing n fingerprints, each represented by m spherical harmonic coefficients (ranging from degree-1 to a certain truncation degree L, with $m = (L+1)^2 - 1$). $\mathbf{X}$ represents the matrix containing k months of scaling factors for each fingerprint. Matrix $\mathbf{b}$ contains k months of GRACE/GRACE-FO gravity field models after the removal of a GIA model. Since $\mathbf{b}$ does not include degree-1 terms and certain coefficients with large uncertainties need to be eliminated, we introduced a truncation matrix $\mathbf{T}$ for the purpose:

$$\underset{m\times m}{\mathbf{T}}\ \underset{m\times k}{\mathbf{b}} = \underset{m\times m}{\mathbf{T}}\ \underset{m\times n}{\mathbf{A}}\ \underset{n\times k}{\mathbf{X}}. \tag{2}$$

For the sake of clarity, let us explain the method with an explicit example. In this example, we considered the case of estimating the degree-1, C_{20}, and C_{30} coefficients simultaneously (a total of five coefficients). We assume that the global gravity field variations observed by GRACE/GRACE-FO can be adequately represented by only four fingerprints generated by mass changes from AIS, Greenland Ice Sheet (GIS), continental glaciers (GLA), and terrestrial water storage (TWS). Additionally, we use two GIA fingerprints to account for the remaining GIA signals. In such a case, Equation 2 can be written as:

$$\underset{m\times m}{\mathbf{T}}\ \underset{m\times k}{\mathbf{b}} = \underset{m\times m}{\mathbf{T}}\ \underset{m\times 6}{\mathbf{A}}\ \underset{6\times k}{\mathbf{X}}, \tag{3}$$

in which the truncation matrix $\mathbf{T}$ is:

$$\mathbf{T} = \begin{array}{c} \begin{matrix} \mathbf{C_{10}} & \mathbf{C_{11}} & \mathbf{S_{11}} & \mathbf{C_{20}} & C_{21} & S_{21} & \mathbf{C_{30}} & C_{31} & \cdots & \cdots & \cdots & \cdots & S_{LM} \end{matrix} \\ \begin{bmatrix} 0 & 0 & 0 & 0 & \mathbf{1} & 0 & 0 & 0 & \cdots & \cdots & \cdots & \cdots & 0 \\ 0 & 0 & 0 & 0 & 0 & \mathbf{1} & 0 & 0 & \ddots & \ddots & \ddots & \ddots & 0 \\ 0 & 0 & 0 & 0 & 0 & 0 & 0 & 0 & \ddots & \ddots & \ddots & \ddots & 0 \\ 0 & 0 & 0 & 0 & 0 & 0 & 0 & \mathbf{1} & \ddots & \ddots & \ddots & \ddots & 0 \\ \vdots & \vdots & \vdots & \vdots & \vdots & \vdots & \vdots & \vdots & \ddots & \ddots & \ddots & \ddots & \vdots \\ \vdots & \vdots & \vdots & \vdots & \vdots & \vdots & \vdots & \vdots & \ddots & \ddots & \ddots & \ddots & \vdots \\ \vdots & \vdots & \vdots & \vdots & \vdots & \vdots & \vdots & \vdots & \ddots & \ddots & \ddots & \ddots & \vdots \\ 0 & 0 & 0 & 0 & 0 & 0 & 0 & 0 & \ddots & \ddots & \ddots & \ddots & 0 \\ 0 & 0 & 0 & 0 & 0 & 0 & 0 & 0 & \cdots & \cdots & \cdots & \cdots & \mathbf{1} \end{bmatrix} \end{array}, \tag{4}$$

where L and M denote the maximum degree and order considered. The coefficients that are being eliminated are shown in red. For a single month, that is, $k = 1$, Equation 3 can be explicitly written as:

$$\underbrace{\begin{bmatrix} C_{21}^{\mathrm{AIS}} & C_{21}^{\mathrm{GIS}} & C_{21}^{\mathrm{GLA}} & C_{21}^{\mathrm{GIA_1}} & C_{21}^{\mathrm{GIA_2}} & C_{21}^{\mathrm{TWS}} \\ S_{21}^{\mathrm{AIS}} & S_{21}^{\mathrm{GIS}} & S_{21}^{\mathrm{GLA}} & S_{21}^{\mathrm{GIA_1}} & S_{21}^{\mathrm{GIA_2}} & S_{21}^{\mathrm{TWS}} \\ C_{22}^{\mathrm{AIS}} & C_{22}^{\mathrm{GIS}} & C_{22}^{\mathrm{GLA}} & C_{22}^{\mathrm{GIA_1}} & C_{22}^{\mathrm{GIA_2}} & C_{22}^{\mathrm{TWS}} \\ S_{22}^{\mathrm{AIS}} & S_{22}^{\mathrm{GIS}} & S_{22}^{\mathrm{GLA}} & S_{22}^{\mathrm{GIA_1}} & S_{22}^{\mathrm{GIA_2}} & S_{22}^{\mathrm{TWS}} \\ C_{31}^{\mathrm{AIS}} & C_{31}^{\mathrm{GRE}} & C_{31}^{\mathrm{GLA}} & C_{31}^{\mathrm{GIA_1}} & C_{31}^{\mathrm{GIA_2}} & C_{31}^{\mathrm{TWS}} \\ \vdots & \vdots & \vdots & \vdots & \vdots & \\ S_{LM}^{\mathrm{AIS}} & S_{LM}^{\mathrm{GIS}} & S_{LM}^{\mathrm{GLA}} & S_{LM}^{\mathrm{GIA_1}} & S_{LM}^{\mathrm{GIA_2}} & S_{LM}^{\mathrm{TWS}} \end{bmatrix}}_{\mathbf{TA}} \underbrace{\begin{bmatrix} x^{AIS} \\ x^{GIS} \\ x^{GLA} \\ x^{GIA_1} \\ x^{GIA_2} \\ x^{TWS} \end{bmatrix}}_{\mathbf{X}} = \underbrace{\begin{bmatrix} C_{21} \\ S_{21} \\ C_{22} \\ S_{22} \\ C_{31} \\ \vdots \\ S_{LM} \end{bmatrix}}_{\mathbf{Tb}}, \tag{5}$$

with the resulting scaling factors in matrix $\mathbf{X}$ we are able to estimate the low-degree coefficients through:

$$\begin{bmatrix} C_{10} \\ C_{11} \\ S_{11} \\ C_{20} \\ C_{30} \end{bmatrix} = \begin{bmatrix} C_{10}^{\mathrm{AIS}} & C_{10}^{\mathrm{GIS}} & C_{10}^{\mathrm{GLA}} & C_{10}^{\mathrm{GIA_1}} & C_{10}^{\mathrm{GIA_2}} & C_{10}^{\mathrm{TWS}} \\ C_{11}^{\mathrm{AIS}} & C_{11}^{\mathrm{GIS}} & C_{11}^{\mathrm{GLA}} & C_{11}^{\mathrm{GIA_1}} & C_{11}^{\mathrm{GIA_2}} & C_{11}^{\mathrm{TWS}} \\ S_{11}^{\mathrm{AIS}} & S_{11}^{\mathrm{GIS}} & S_{11}^{\mathrm{GLA}} & S_{11}^{\mathrm{GIA_1}} & S_{11}^{\mathrm{GIA_2}} & S_{11}^{\mathrm{TWS}} \\ C_{20}^{\mathrm{AIS}} & C_{20}^{\mathrm{GIS}} & C_{20}^{\mathrm{GLA}} & C_{20}^{\mathrm{GIA_1}} & C_{20}^{\mathrm{GIA_2}} & C_{20}^{\mathrm{TWS}} \\ C_{30}^{\mathrm{AIS}} & C_{30}^{\mathrm{GIS}} & C_{30}^{\mathrm{GLA}} & C_{30}^{\mathrm{GIA_1}} & C_{30}^{\mathrm{GIA_2}} & C_{30}^{\mathrm{TWS}} \end{bmatrix} \begin{bmatrix} x^{\mathrm{AIS}} \\ x^{\mathrm{GIS}} \\ x^{\mathrm{GLA}} \\ x^{\mathrm{GIA1}} \\ x^{\mathrm{GIA2}} \\ x^{\mathrm{TWS}} \end{bmatrix}. \tag{6}$$

In practice, a time-domain constraint is applied to ensure the linearity of the GIA signals:

$$\frac{\chi_{m_k}^{GIA} - \chi_{m_{k-1}}^{GIA}}{m_k - m_{k-1}} = \frac{\chi_{m_{k+1}}^{GIA} - \chi_{m_k}^{GIA}}{m_{k+1} - m_k}, \tag{7}$$

where m_k denotes the kth month, and m_{k-1} and m_{k+1} are the previous and following months, respectively. Note that the equation does not require the months to be continuous. To implement this constraint, we need to construct a large block diagonal matrix to solve all monthly solutions simultaneously. In Figure 1, we show how this works with a specific example of 4 months.

In this section, we have provided a specific example based on an oversimplified scenario. In the following, as we introduce the actual input data and the fingerprint database, we will assign realistic parameters to Equation 2 to bridge the simplified example with a realistic scenario.

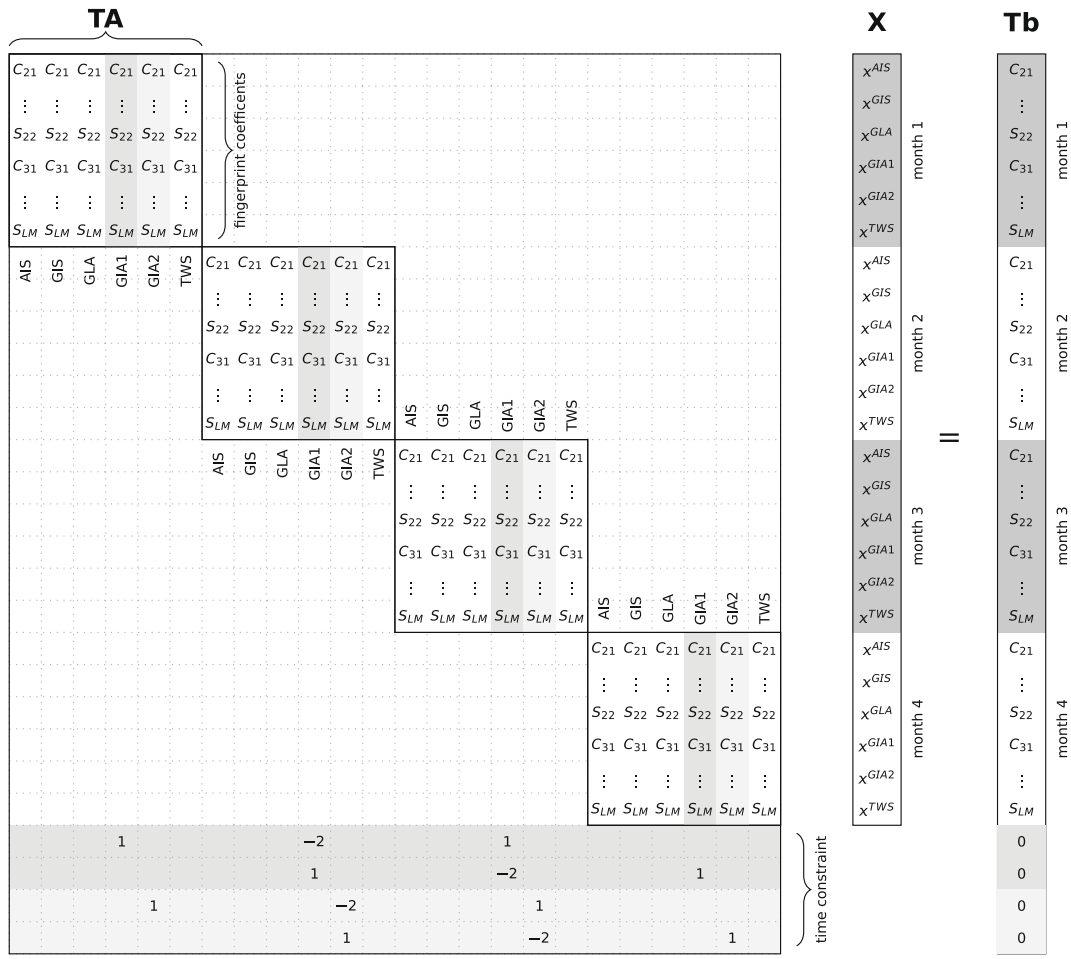

Figure 1. Scheme of implementing the time domain constraint on residual Glacial Isostatic Adjustment (GIA) contributions. We show the case of only four monthly GRACE/GRACE-FO gravity field models, six fingerprints. The time domain constraint on the GIA contributions is introduced by adding rows below the design matrix to make sure that resulting GIA scalars (x^{GIA1}, x^{GIA2}) satisfy Equation 7.

2.2. GRACE/GRACE-FO Data

The Level-2 GRACE/GRACE-FO gravity field models are officially made available by three data centers: the Center for Space Research at the University of Texas at Austin (CSR), the Jet Propulsion Laboratory (JPL), and the German Research Center for Geosciences (GFZ) (Bettadpur, 2007; Dahle et al., 2019; Landerer et al., 2020).

For the spherical harmonic coefficients in the vector $\mathbf{b}_{(m\times k)}$ of Equation 2, we utilized data from all three official processing centers: CSR, GFZ, and JPL. During the GRACE mission, we employed the RL06 solutions, while for the GRACE-FO period, we used the latest available releases−RL06.3 for CSR, JPL, and GFZ. These solutions cover a period of over two decades from April 2002 to July 2024 (accessed in November 2024). A mean gravity field and a GIA model (e.g., ICE6G-D) were removed to obtain time variations of monthly gravity fields due to surface mass changes. We use the unfiltered solutions and do not apply any smoothing or filtering techniques to avoid signal distortions. In the main text, we present results from the CSR solution, with similar results from the other two solutions documented in Supporting Information S1.

Since all the gravity field solutions are complete up to degree 60, m equals 3,720 (with the three degree-1, C_{20}, and C_{30} coefficients padded with zeros), and k is 235 in our case.

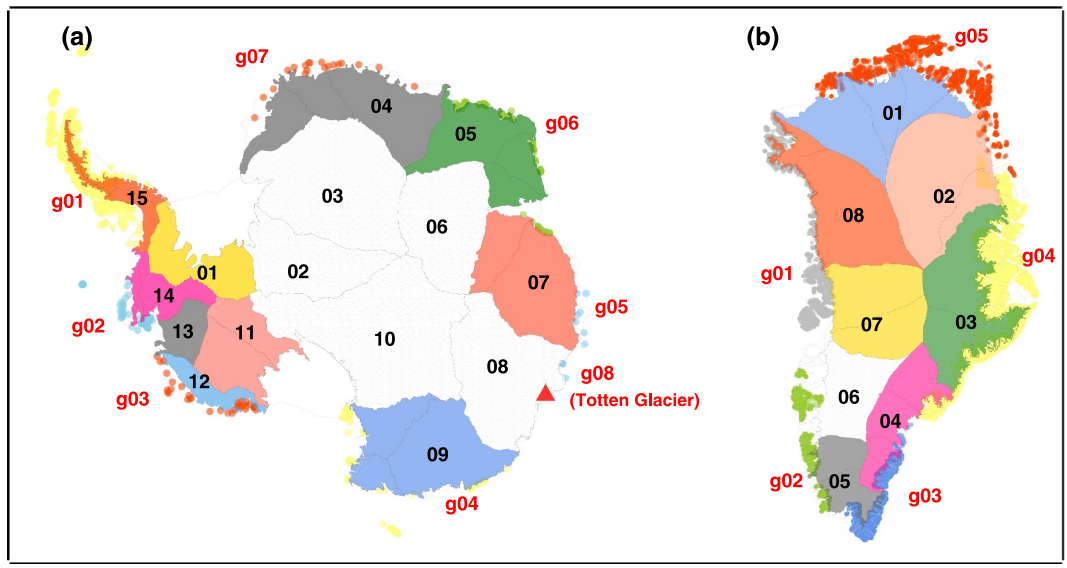

Figure 2. Selected scheme for dividing the Antarctic Ice Sheet (a) and Greenland Ice Sheet (b) into blocks. The gray lines represent the drainage system provided by Zwally et al. (2005), with merged basins shown in the same filled colors. Peripheral glaciers are marked as colored points.

2.3. Fingerprint Database

The construction of the fingerprint database has been described in a series of previous studies (Rietbroek et al., 2016; Sun & Riva, 2020; Sun et al., 2019). Here, the GLA and TWS fingerprints are the same as those used in Sun and Riva (2020). The GLA positions are provided by the World Glacier Inventory/Global Land Ice Measurement from Space (WGI/GLIM) data set. We classified the listed glaciers into 34 clusters (Figure S1 in Supporting Information S1), each representing a unit (one-gigaton) total mass change, assuming a spatial pattern proportional to the number of glaciers present. The TWS modes are based on the empirical orthogonal function analysis of the WaterGAP hydrology model v2.2d (Müller Schmied et al., 2021) excluding the glaciated areas. The 60 leading EOFs, along with three additional fingerprints for the Caspian Sea, the North India Plain, and Lake Victoria, are employed.

For the AIS and GIS, we generated fingerprints based on mass change blocks defined by two widely used drainage basin systems (Rignot & Mouginot, 2012; Zwally et al., 2005). Note that we selectively merged several neighboring drainage basins to form larger blocks, as some basins are smaller than the native resolution of GRACE/GRACE-FO. Our simulations using synthetic input (see Supporting Information S1) demonstrate that the block dividing scheme has minor effects on the results for estimating low-degree coefficients (see Figure S3 in Supporting Information S1). However, we kept most of the small basins over West Antarctica separated to reflect the actual mass change. Additionally, we created fingerprints for peripheral glaciers (five for Greenland and seven for Antarctica) using the WGI/GLIMS data set. We also included a specific fingerprint for the Totten Glacier in East Antarctica due to its significant mass changes, following Sun et al. (2019). Ultimately, we employed 23 and 13 fingerprints for the AIS and GIS, respectively (Figure 2).

Besides surface mass changes, the remaining GIA signals after the removal of the a priori GIA model (e.g., ICE6G-D) must be considered, in view of the large uncertainties carried by GIA models. In this study, we employed six GIA fingerprints to account for these residual signals. These fingerprints correspond to those employed by Sun and Riva (2020), encompassing one for the entirety of Antarctica, two for Northern Europe, and three for North America.

Finally, we prepared a fingerprint database comprising a total of 139 fingerprints. Each fingerprint was converted to spherical harmonic coefficients, arranged in vectors to form the matrix $\mathbf{A}_{(m\times n)}$ as defined in Equation 2. Here, n representing the number of fingerprints, equals 139. At this point, we are prepared to solve for the matrix $\mathbf{X}$ according to Equation 2.

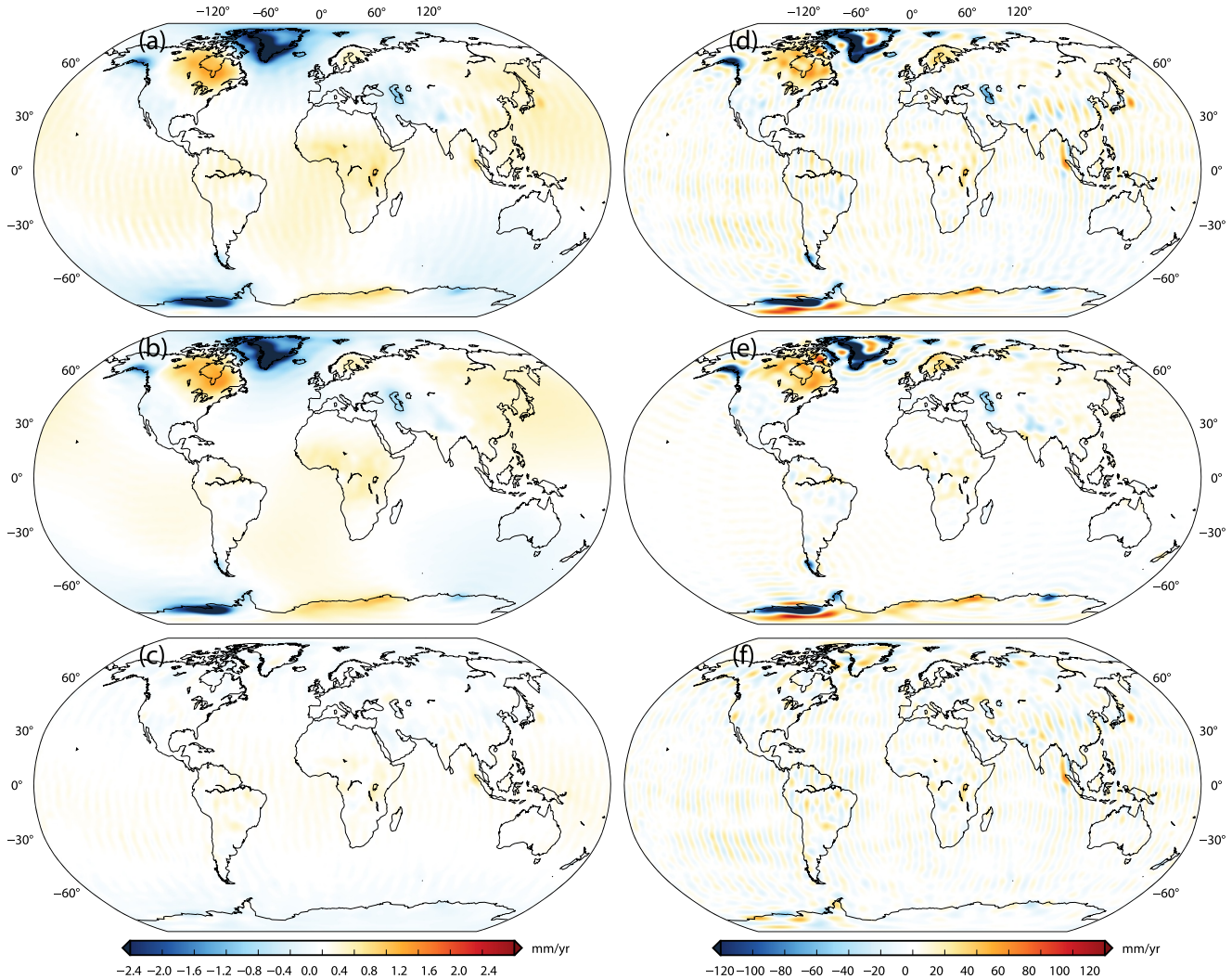

Figure 3. Global trend map in terms of geoid ((**a**), (**b**), (**c**)) and equivalent water height ((**d**), (**e**), (**f**)). Panels (**a**) and (**d**) show the results recovered with the original CSR RL06 solution. Panels (**b**) and (**e**) show those based on the fingerprint approach. Panels (**c**) and (**f**) show the residual signals between the two solutions ((**a**), (**b**) and (**d**), (**e**)). Notice the different color scales.

3. Results

3.1. Validation of Fingerprint Database for Representing Observed Mass Changes

In this section, we aim to assess whether the prescribed blocks/modes and the resulting fingerprint database adequately represent the mass changes observed by the GRACE/GRACE-FO missions. To verify this, we compared the global geoid and equivalent water height trends derived from the original GRACE/GRACE-FO solutions (degree-1 coefficients are ignored, C_{20} and C_{30} coefficients are replaced by those from TN-14) with those reconstructed from the fingerprints (Figure 3). The residuals are generally small, except for the coseismic signals from mega-thrust earthquakes and ice mass loss from West Antarctica. Such deviations are expected, as the database does not include earthquake-related fingerprints, and the large gradients in West Antarctica may not be well captured by the uniform mass variations assigned to the drainage systems. However, these signals should have a minimal effect on the estimated low-degree coefficients due to their limited spatial extent.

Since all fingerprints are normalized to a one-gigaton mass change, the scaling factors (see matrix **X** in Equation 2) should estimate their total mass change. By summing the scaling factors associated with the Antarctica and Greenland mass change blocks, we can estimate the total mass change over there. In Figure 4, we compare this result with those from the Ice sheet Mass Balance Inter-comparison Exercise (IMBIE) (Otosaka et al., 2023), as

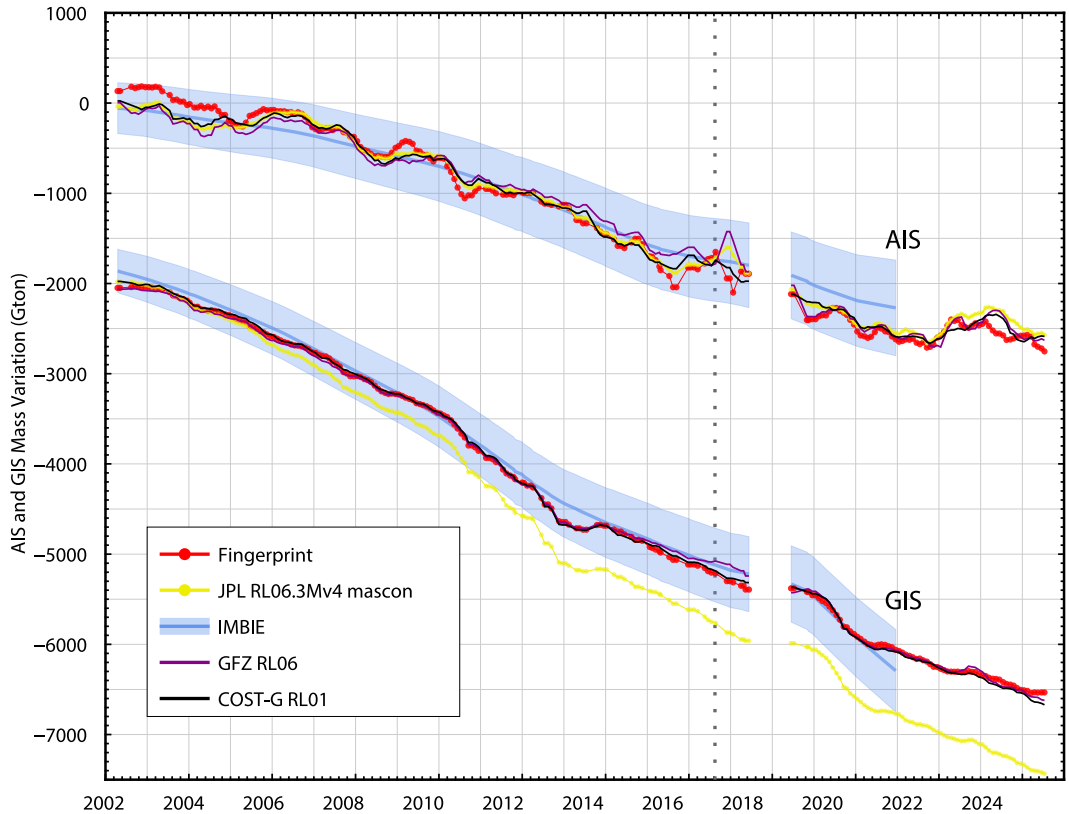

Figure 4. Estimated Antarctic Ice Sheet and Greenland Ice Sheet mass change time series based on **X** using the fingerprint approach, compared to results from the IMBIE and several GRACE/GRACE-FO-based solutions. Note that we removed the periodic signals from the fingerprint method and the GRACE/GRACE-FO results, subtracted their mean over a common reference period (from April 2002 to July 2016), and use a half-year sliding window to smooth these time series to better compare with the IMBIE results.

well as several GRACE/GRACE-FO-based solutions, including the JPL RL06.3Mv4 mascon (Wiese & Yuan, 2024), GFZ RL06 (Sasgen et al., 2019), and the International Combination Service for Time-variable Gravity (COST-G) RL01 (Sasgen et al., 2020). The IMBIE solution provides reconciled mass balance estimates based on three independent satellite techniques: altimetry, gravimetry, and the input-output method, excluding seasonal signals. For a better comparison with IMBIE, we removed the periodic signals from both our fingerprint estimates and the GRACE/GRACE-FO results, smoothing the resulting time series with a half-year running mean. Our estimates closely align with all solutions for both the AIS and GIS, except for the JPL RL06.3Mv4 mascon solution over the GIS. The comparatively larger trend observed in the JPL RL06.3Mv4 mascon solution for the GIS may be attributed to its consideration of Earth's oblateness, which tends to yield higher mass change estimates (e.g., Ditmar, 2018; Ghobadi-Far et al., 2019; Li et al., 2017). Nevertheless, this difference remains within the current uncertainty (about 40 Gt/yr) in GIS mass change estimates (see Table 2 of Otosaka et al. (2022)).

3.2. Degree-1 Coefficients

In Figure 5, we show three degree-1 time series derived from the fingerprint approach. Additionally, we present two other solutions for comparative purposes. One solution is the recommended degree-1 documented in technique note 13 (TN-13) (from April 2002 to April 2024), while the other is derived following Sun et al. (2023). Both comparative solutions are based on the GRACE-OBP approach but differ in implementation details. Specifically, we estimated the degree-1, C_{20}, and C_{30}. In contrast, TN-13 focuses solely on the degree-1 coefficients. However, such a difference should not lead to significant differences in the degree-1 coefficients (Sun et al., 2023). Another distinction is our use of a narrower (200 km compared to 300 km) buffer width to exclude ocean areas potentially contaminated by continental signals. Notably, the difference in the estimated linear trend

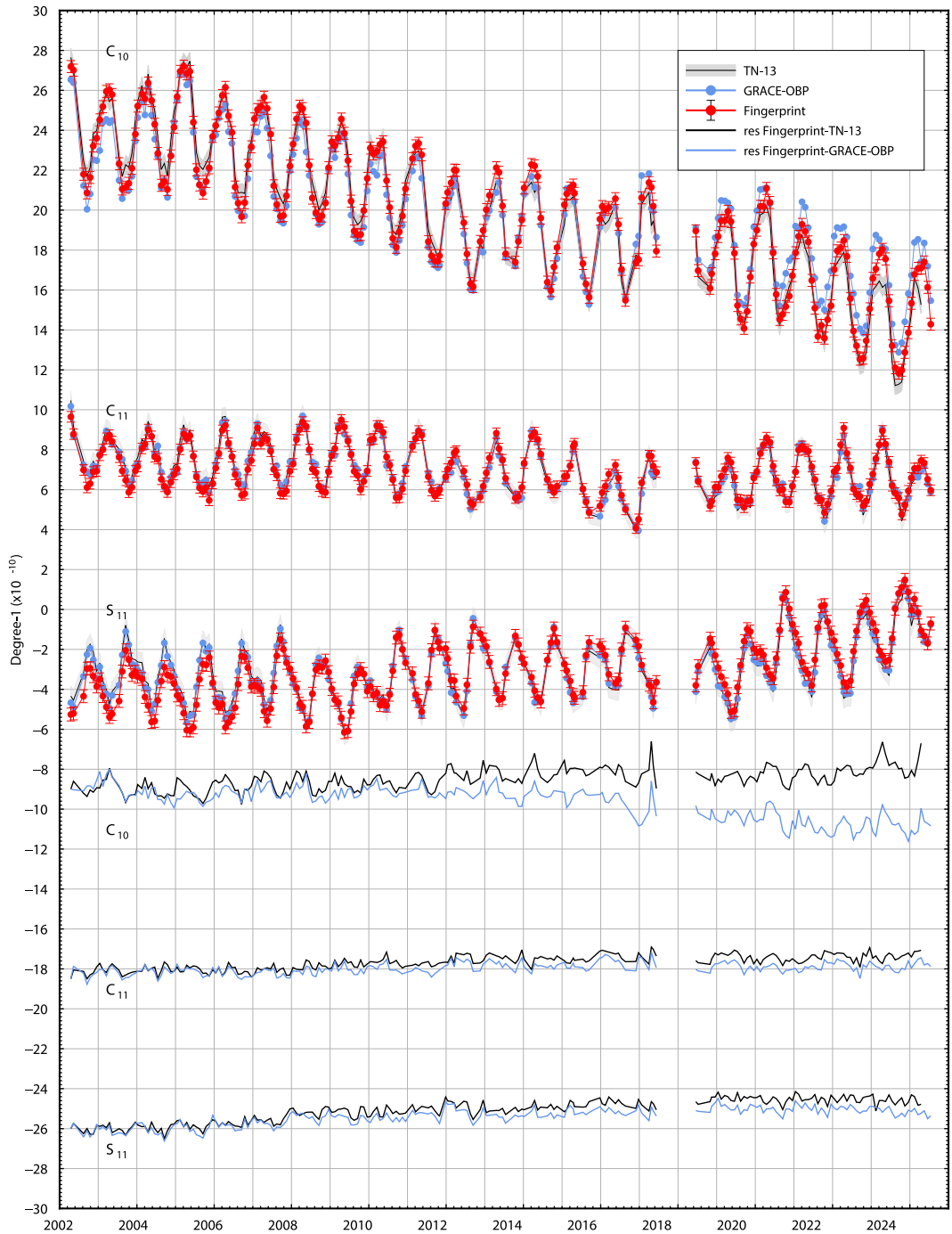

Figure 5. Comparison of estimated degree-1 time series from different approaches. The estimated degree-1 time series from the fingerprint approach is shown as the red curve with solid dots, where the error bars represent the standard deviation (STD) of the random noise in our time series, estimated according to Equation (8) in Ditmar (2022). We compared our solution to the recommended TN-13 solution (black curve), with the provided error estimates displayed as a gray band. Additionally, we compared our results to the GRACE-OBP solution in house, shown as the blue curve with solid dots. Residual time series are also presented, illustrating the differences between our estimates and those from both TN-13 and GRACE-OBP.

C_{10} values is smaller (see Table 1). We verified that using a 300 km buffer width yields results consistent with TN-13. The GRACE-OBP method relies on model-predicted OBP data to determine the degree-1 coefficients, and using a narrower buffer increases the amount of OBP data, which is beneficial. It also amplifies the solution's sensitivity to large land-mass changes, particularly from Antarctica and Greenland. By bringing the ocean data

Table 1
Estimated Annual Amplitude, Phase, and Linear Trends of Degree-1 Coefficient Time Series

Coefficients	Approach	Amp (10^{-11})	Amp (mm)	Pha (days)	Trnd (10^{-11}yr^{-1})	Trnd (mm yr^{-1})	Time span
C_{10}	TN-13	24.0 ± 1.0	2.6 ± 0.1	83 ± 2	−4.8 ± 0.1	−0.52 ± 0.01	2002.04–2024.04
	GRACE-OBP	25.9 ± 0.7	2.8 ± 0.1	77 ± 2	−3.6 ± 0.1	−0.39 ± 0.01	2002.04–2024.07
	Fingerprint	27.9 ± 0.6	3.0 ± 0.1	80 ± 1	−4.4|−5.0 ± 0.1	−0.48|−0.54 ± 0.01	
	Fingerprint ALT	26.1 ± 0.7	2.8 ± 0.1	83 ± 1	−4.6|−5.1 ± 0.1	−0.49|−0.56 ± 0.01	2002.04–2023.05
C_{11}	TN-13	13.7 ± 0.6	1.5 ± 0.1	100 ± 2	−1.0 ± 0.1	−0.11 ± 0.01	2002.04–2024.04
	GRACE-OBP	12.9 ± 0.6	1.4 ± 0.1	101 ± 2	−0.8 ± 0.1	−0.09 ± 0.01	2002.04–2024.07
	Fingerprint	14.4 ± 0.5	1.6 ± 0.1	99 ± 2	−0.6|−0.8 ± 0.1	−0.06|−0.08 ± 0.01	
	Fingerprint ALT	14.4 ± 0.5	1.6 ± 0.1	100 ± 2	−0.6|−0.8 ± 0.1	−0.07|−0.08 ± 0.01	2002.04–2023.05
S_{11}	TN-13	15.8 ± 0.6	1.7 ± 0.1	62 ± 2	0.7 ± 0.1	0.08 ± 0.01	2002.04–2024.04
	GRACE-OBP	15.9 ± 0.6	1.7 ± 0.1	66 ± 2	1.0 ± 0.1	0.11 ± 0.01	2002.04–2024.07
	Fingerprint	15.2 ± 0.5	1.7 ± 0.1	59 ± 2	1.5|2.0 ± 0.1	0.17|0.21 ± 0.01	
	Fingerprint ALT	15.5 ± 0.5	1.7 ± 0.1	60 ± 2	1.5|1.9 ± 0.1	0.16|0.21 ± 0.01	2002.04–2023.05

Note. The error estimates represent formal errors obtained from the post-fit least squares. Atmospheric and oceanic contributions are excluded.

closer to land, the narrower buffer increases responsiveness to mass changes over land due to self-gravitation and loading effects. Hereafter, any mention of the GRACE-OBP solution in the main text and captions refers to the version produced using our own parameter settings, unless otherwise specified.

The estimated annual amplitude, phase, and linear trend of the degree-1 coefficients show minimal variations between TN-13 and the GRACE-OBP solution developed in this study. The only notable difference is that the GRACE-OBP solution exhibits a relatively smaller linear trend for C_{10} (0.39 mm/yr compared to 0.52 mm/yr). Note that we convert the dimensionless degree-1 coefficients into geocenter motions in mm following Equation (2) from Sun, Riva, and Ditmar (2016). Compared to these two solutions, the fingerprint approach yields annual amplitude and phase estimates that are very similar for both C_{11} and S_{11} (annual amplitudes are within two sigma, and phases differ by less than 1 week), which represent the X and Y components of geocenter motion. For C_{10}, the Z component of geocenter motion, the fingerprint approach produces a slightly larger annual amplitude compared to the other two solutions, corresponding to a geocenter motion of approximately 3 mm, compared to 2.6 and 2.8 mm for the other solutions. The phase estimates for C_{10} are again quite similar, differing by less than 1 week.

Among the three coefficients, only C_{10} exhibits a relatively prominent linear trend, primarily driven by the substantial mass loss from the GIS, which exceeds the mass loss from the AIS. This north-south imbalance results in a long-term redistribution of mass toward the Southern Hemisphere, a process further amplified by the significantly larger oceanic coverage in the Southern Hemisphere compared to the Northern Hemisphere. The fingerprint approach's C_{10} linear trend falls between the estimates from TN-13 and GRACE-OBP. For the other two coefficients, where the linear trends have much smaller magnitudes, the fingerprint approach shows a slightly smaller trend for C_{11} and a slightly larger trend for S_{11}, but both remain within 0.1 mm/yr.

Additionally, we present statistics for a solution based on the fingerprint approach that combines altimetry data (Fingerprint ALT) (see Text S3 in Supporting Information S1). Compared to the solution using only GRACE/GRACE-FO data, the largest discrepancy is observed in the C_{10} annual amplitude estimates, differing by approximately 10% (2.8 mm compared to 3.0 mm). In Table 1, we present results from the fingerprint approach using Caron GIA model (Caron et al., 2018), where Caron GIA model is removed instead of ICE6G-D prior to implementing the approach. In the table, the linear trends computed based on the Caron GIA model are highlighted in blue in the table. Notably, the annual variations remain consistent between the results derived from both GIA models. As expected, using a different GIA model impacts only the linear trend estimates, with minor differences observed (within 0.1 mm/yr).

3.3. C_{20} Coefficients

We present our C_{20} solution derived from the fingerprint approach in Figure 6. Additionally, we display a solution based on the GRACE-OBP approach and two solutions based on SLR data processing. Their annual amplitudes,

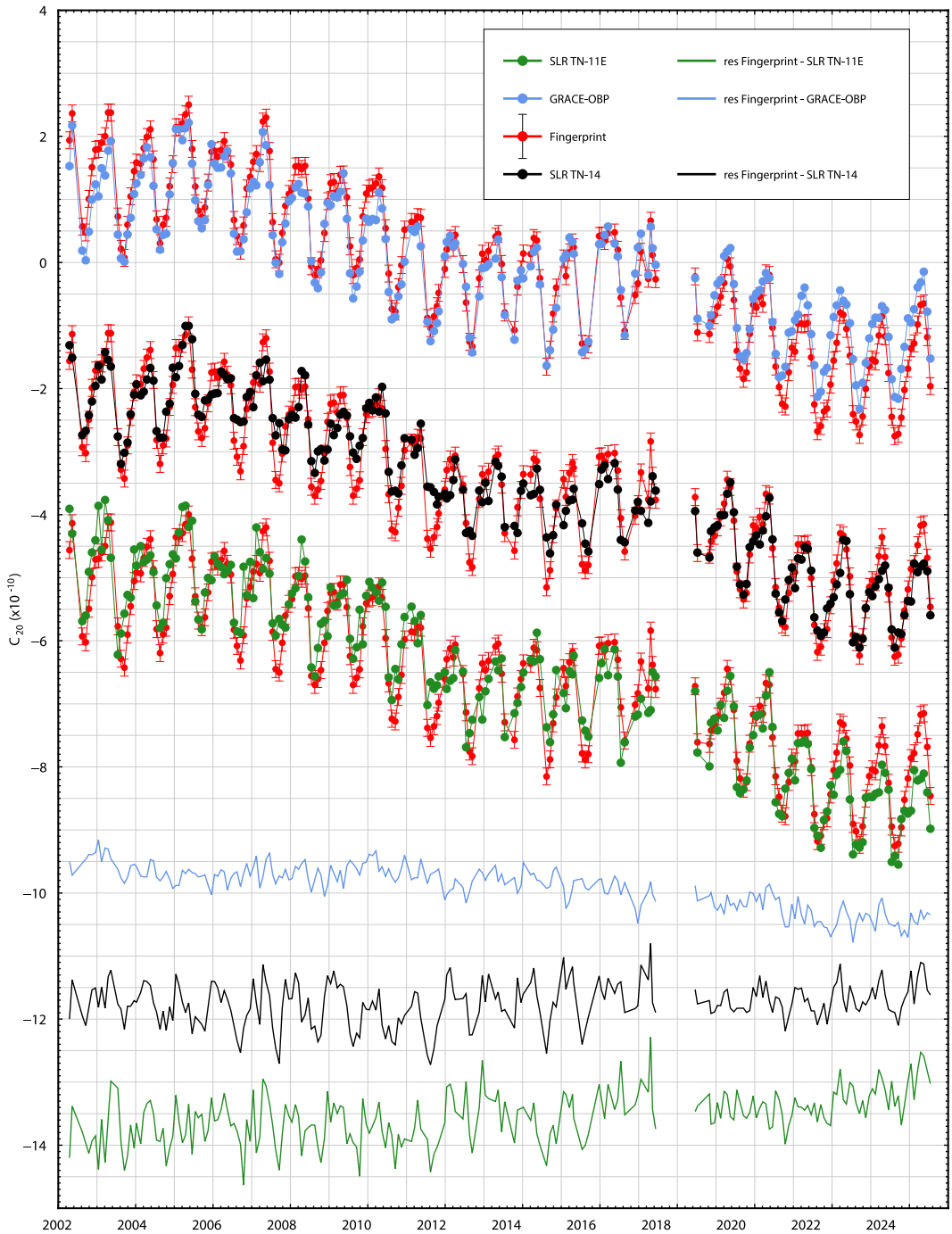

Figure 6. Estimated C_{20} time series based on the fingerprint approach, GRACE-OBP approach, and two SLR-based solutions. The fingerprint results are depicted by the red curve with solid dots. For clarity, the fingerprint solution is intentionally shifted to facilitate comparison with the GRACE-OBP solution (blue curve), Satellite Laser Ranging (SLR) TN-14 (black curve), and SLR TN-11E (green curve). Error bars for the fingerprint and GRACE-OBP approaches represent the standard deviation of random noise in the time series, estimated following Ditmar (2022).

phases, and linear trend estimates are summarized in Table 2. The C_{20} time series from the fingerprint approach correlates particularly well with the GRACE-OBP solution, with the annual amplitude estimates within uncertainties, and phases differing by only 2 days. However, the fingerprint approach shows a larger linear trend which aligns more closely with the SLR solutions. The recommended replacements for the original GRACE/GRACE-FO C_{20} coefficients are based on SLR data processing. Specifically, the SLR TN-14 solution (Loomis

Table 2
Estimated Annual Amplitudes, Phases, and Linear Trends of C_{20} Time Series

	C_{20}			
Approach	Amp (10^{-11})	Pha (days)	Trnd (10^{-11}yr^{-1})	Time span
GRACE-OBP	7.9 ± 0.4	75 ± 2	−1.3 ± 0.1	2002.04–2024.07
SLR TN-11E	6.1 ± 0.4	74 ± 3	−1.9 ± 0.1	
SLR TN-14	5.3 ± 0.3	85 ± 3	−1.7 ± 0.1	
Fingerprint	8.3 ± 0.3	77 ± 2	−1.7|−1.3 ± 0.1	
Fingerprint ALT	6.8 ± 0.3	84 ± 2	−2.0|−1.5 ± 0.1	2002.04–2023.05

et al., 2020) replaced TN-11 as the standard C_{20} solution since 2020. The SLR TN-11E is an updated version of TN-11 by combining data from seven SLR satellites (Cheng & Ries, 2023). While the linear trends of the two SLR solutions differ by approximately 10%, their annual amplitudes show a slightly larger discrepancy (around 15%, $6.1 \pm 0.3 \times 10^{-11}$ for SLR TN-11E and $5.3 \pm 0.3 \times 10^{-11}$ for SLR TN-14). Note that TN-11E has been updated since its initial publication, and its estimated annual amplitude has changed since Cheng and Ries (2023). The annual amplitude of our solution ($8.3 \pm 0.3 \times 10^{-11}$) is nearly identical to that of SLR TN-11E. Including altimetry data in the fingerprint approach reduces the annual amplitude by approximately 20% while increasing the linear trend by about 20%. Conversely, using a different GIA model (Caron) in the fingerprint approach reduces the linear trend by approximately 25%.

3.4. C_{30} Coefficients

We compare C_{30} solutions in Figure 7. Annual amplitudes, phases, and linear trends for three distinct time periods are computed and summarized in Table 3. During the first period (April 2002 to February 2012), a 10-year nominal phase, we compare our solution with those from the original GRACE and the GRACE-OBP approach. All three solutions exhibit nearly identical annual phases (within 10 days). However, notable differences are observed in annual amplitudes: the C_{30} amplitudes from the GRACE-OBP approach are approximately 20% larger than those from the original GRACE/GRACE-FO C_{30} time series. The fingerprint approach, on the other hand, falls between the two solutions but is closer to the GRACE-OBP approach (also true for the other two periods).

The second period (March 2012 to July 2016), also within the nominal phase, spans slightly over 4 years. During this period, the seasonal signals of the three GRACE-based solutions remain consistent with those observed in the first period. Additionally, we include two SLR-based solutions for comparison. The SLR-based C_{30} solutions are expected to be more accurate since the launch of the LAser RElativity Satellite (LARES) in March 2012, due to its high sensitivity to C_{30}. The SLR-based solutions, TN-14 and TN-11E, show a high level of consistency with the original GRACE C_{30} solution, although their amplitude estimates are approximately 15% and 20% lower, respectively, than those derived from GRACE. This discrepancy means that the fingerprint approach differs even more from the SLR solutions. For example, the difference in amplitude estimates between the fingerprint approach and the TN-14 is about 25%.

The third period begins in August 2016, spanning the degraded interval. During this period, the original GRACE/GRACE-FO C_{30} coefficients are considered to be less reliable. The solutions based on the fingerprint approach and the GRACE-OBP approach show similar seasonal signal statistics to those of the previous two periods. However, the amplitude estimates of the SLR-based solutions are slightly larger (within 10%) than the GRACE-based results but remain significantly smaller than those obtained from the fingerprint approach and the GRACE-OBP approach. Over all three periods, incorporating altimetry data generally reduces the amplitude.

We provide linear trend estimates for the first and third periods in Table 3. Linear trends for the second period are not shown due to the time span being too short for reliable estimation. Notably, C_{30} from the fingerprint approach consistently shows a slightly steeper trend compared to other solutions, particularly the GRACE-OBP solution. However, there is no visually significant difference when compared to the TN-14 solution (see residuals in Figure 7). Substituting the Caron GIA model for ICE6G-D in the fingerprint approach has minimal impact on the linear trend in the C_{30} time series.

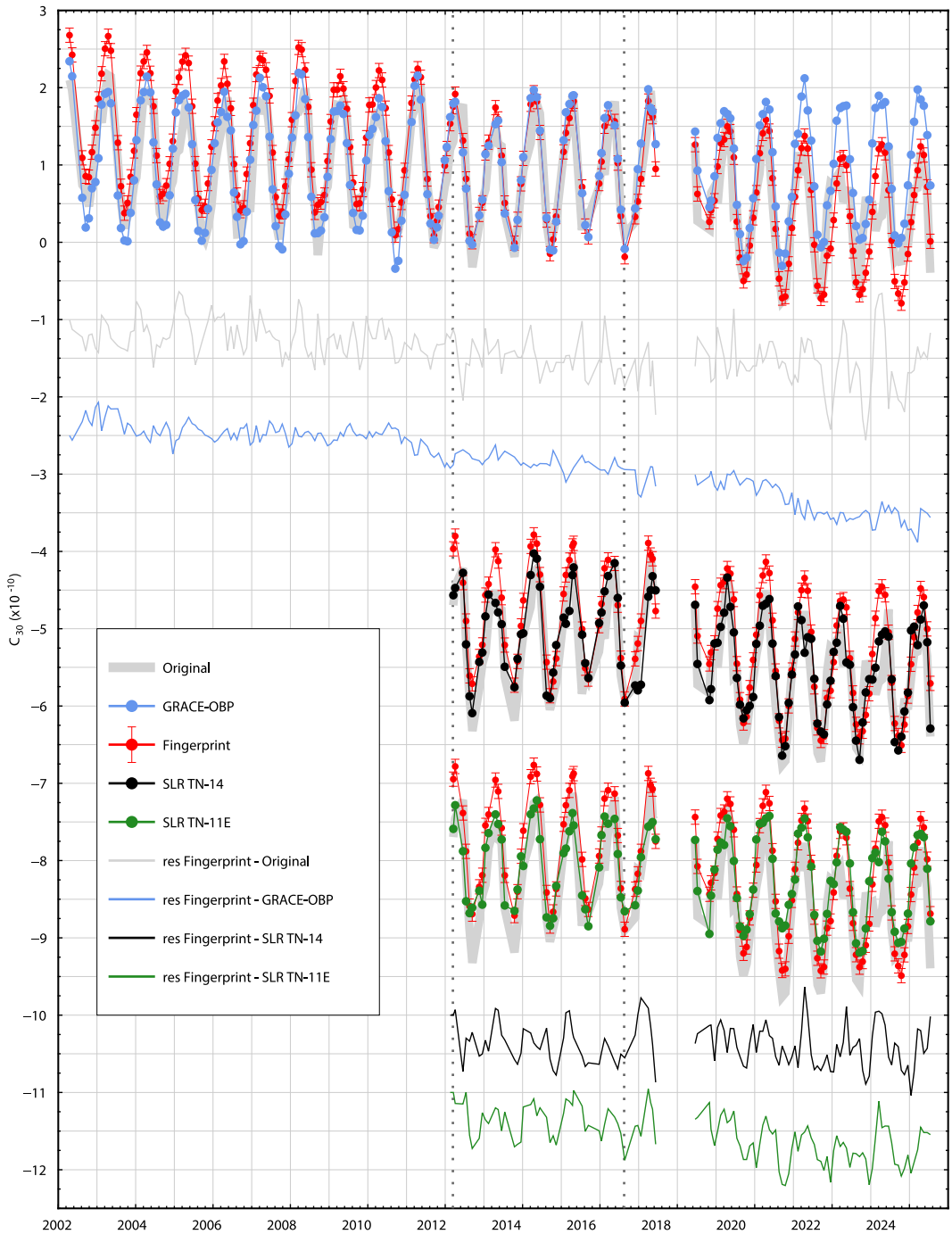

Figure 7. C_{30} time series based on the fingerprint approach, GRACE-OBP approach, and two SLR-based solutions. The fingerprint results are depicted by the red curve with solid dots. To facilitate comparison, the fingerprint solution is intentionally shifted to facilitate comparison with the original GRACE/GRACE-FO solution (thick gray curve), GRACE-OBP solution (blue curve), Satellite Laser Ranging (SLR) TN-14 (black curve), and SLR TN-11E (green curve). Error bars for the fingerprint approaches represent the standard deviation of random noise in the time series, estimated following Ditmar (2022). The two dotted lines indicate the start of the LARES mission and the onset of the degraded period, respectively.

Table 3
Estimated Annual Amplitudes, Phase, and Linear Trends of C_{30} Time Series for Various Time Spans

	C_{30}			
Approach	Amp (10^{-11})	Pha (days)	Trnd (10^{-11}yr^{-1})	Time span
GRACE/GRACE-FO	8.4 ± 0.2	97 ± 2	−0.3 ± 0.1	2002.04–2012.02
GRACE-OBP	9.9 ± 0.2	87 ± 1	−0.2 ± 0.1	
Fingerprint	9.7 ± 0.2	90 ± 1	−0.5|−0.4 ± 0.1	
Fingerprint ALT	9.0 ± 0.2	95 ± 1	−0.5|−0.5 ± 0.1	
GRACE/GRACE-FO	8.4 ± 0.5	98 ± 4	/	2012.03–2016.07
GRACE-OBP	9.7 ± 0.3	89 ± 2	/	
SLR TN-11E	6.9 ± 0.4	85 ± 3	/	
SLR TN-14	7.2 ± 0.5	90 ± 4	/	
Fingerprint	9.3 ± 0.3	92 ± 1	/	
Fingerprint ALT	8.5 ± 0.3	101 ± 2	/	
GRACE/GRACE-FO	7.4 ± 0.5	84 ± 3	−1.0 ± 0.2	2016.08–2024.07
GRACE-OBP	9.9 ± 0.2	89 ± 1	−0.1 ± 0.1	
SLR TN-11E	7.6 ± 0.2	87 ± 2	−0.3 ± 0.1	
SLR TN-14	8.0 ± 0.4	92 ± 3	−0.5 ± 0.1	
Fingerprint	9.8 ± 0.2	93 ± 1	−0.9|−0.8 ± 0.1	
Fingerprint ALT	9.0 ± 0.3	98 ± 2	−1.4|−1.3 ± 0.1	2016.08–2023.05

3.5. The Impact of Low-Degree Coefficients on AIS Mass Change Estimates

Low-degree coefficients play a pivotal role in estimating mass changes, particularly at the poles. In this section, we use AIS as an example to evaluate the cumulative effect of replacing different sets of low-degree coefficients. Figure 8 shows AIS mass change time series derived from CSR RL06.3 gravity field solutions with different low-degree coefficients replaced and compares them to a from IMBIE (also shown in Figure 4). Consistent post-processing procedures were applied, including the destriping technique by Duan et al. (2009), an improved Swenson decorrelation filter (Swenson & Wahr, 2006), 300 km Gaussian smoothing, and a 300 km buffer to account for ocean signal leakage.

In Table 4, we compare the solutions for annual variations across the nominal and degraded periods. During the nominal period, the combined impact of our fingerprint approach for degree-1, C_{20}, and C_{30} is comparable to the currently recommended solution (TN-13 for degree-1, TN-14 for C_{20} and C_{30}) as well as the GRACE-OBP approach. The annual amplitude estimates are similar, differing by less than 10 Gt. During the degraded period, these three solutions remain close, though they yield slightly larger amplitude estimates compared to the nominal period (25–50 Gt higher). The phase estimates of TN-14 differ by 27 days across both periods, while the phase estimates of the GRACE-OBP approach and our fingerprint approach differ by less than 10 days across both periods.

For linear trend estimates, different solutions vary by about 10 Gt/yr during the nominal period. However, in the degraded period, discrepancies increase up to 30 Gt/yr. Specifically, the TN-14 solution and the fingerprint approach differ by about 6 Gt/yr, while both are approximately 20–30 Gt/yr lower than the TN-11E and GRACE-OBP solutions. To avoid potential bias from time series with changing trends before 2007 and after 2022, we calculated trends for a shortened nominal period starting in 2007 and a shortened degraded period ending in 2022. In these shortened periods, the solutions from the fingerprint approach align more closely with those using SLR solutions for C_{20} and C_{30}. Conversely, the GRACE-OBP method exhibits a higher linear trend, approximately 15–20 Gt/yr higher than the other methods. However, we observed significantly different annual amplitudes, with the latter period showing nearly double the amplitude of the former. A closer inspection of the time series reveals that the AIS mass change annual amplitude was larger before 2007 and after 2016, but noticeably smaller during 2007–2016. The reason for this discrepancy remains unclear.

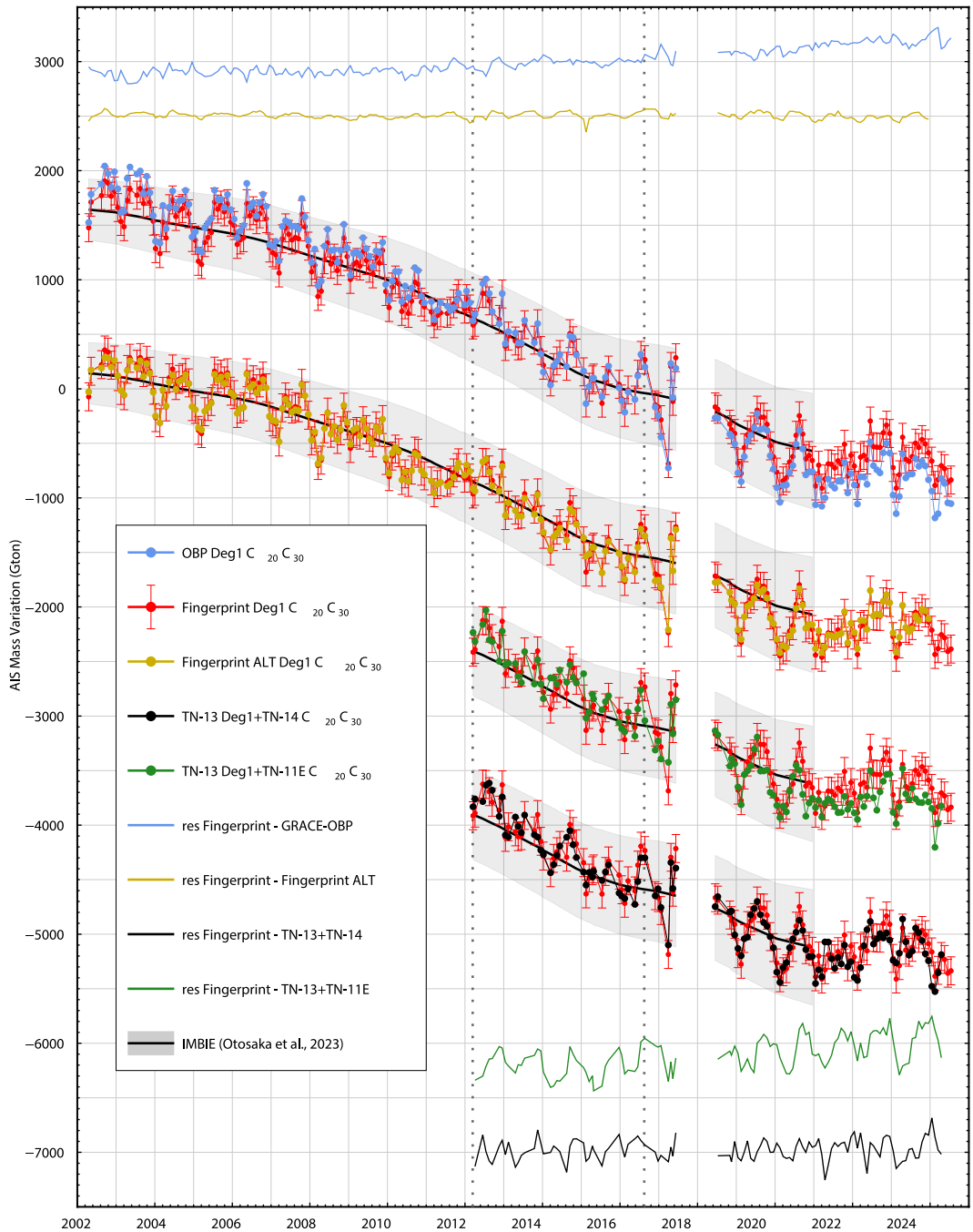

Figure 8. Estimated Antarctic Ice Sheet mass change based on different low-degree coefficients.

Finally, we evaluated the impact of low-degree coefficients from the fingerprint approach using two different GIA models, which led to linear trend differences within 5 Gt/yr. Incorporating altimetry data did not affect the linear trend estimates but resulted in a significant underestimation of the annual amplitude.

4. Discussion and Conclusions

Our results demonstrate that the degree-1, C_{20}, and C_{30} coefficients derived from the fingerprint approach are comparable to the recommended solutions (TN-13 for degree-1 and TN-14 for C_{20} and C_{30}). The differences are negligible for estimating mass changes over the AIS. Thus, these coefficients can reliably supplement or replace

Table 4
Annual Amplitudes, Phases, and Trends of Different Approaches in Antarctic Ice Sheet Mass Change Time Series

Approach	Annual variations			Time span
	Amp(Gt)	Pha (days)	Trnd (Gt yr^{-1})	
TN-13 *Deg*1 + TN-14 C_{20} C_{30}	126.6 ± 10.9	241 ± 5	−127.2 ± 2.0	2002.04–2016.07
TN-13 *Deg*1 + TN-11E C_{20} C_{30}	113.0 ± 13.9	226 ± 7	−131.8 ± 2.5	
GRACE-OBP *Deg*1 C_{20} C_{30}	133.4 ± 15.8	240 ± 7	−132.7 ± 2.9	
Fingerprint *Deg*1 C_{20} C_{30}	133.9 ± 14.4	249 ± 6	−124.1|−120.0 ± 2.6	
Fingerprint ALT *Deg*1 C_{20} C_{30}	111.2 ± 14.7	253 ± 7	−123.1|−119.2 ± 2.7	
TN-13 *Deg*1 + TN-14 C_{20} C_{30}	171.1 ± 20.0	214 ± 7	−65.7 ± 9.9	2016.08–2024.04
TN-13 *Deg*1 + TN-11E C_{20} C_{30}	117.7 ± 21.4	208 ± 11	−84.1 ± 10.6	
GRACE-OBP *Deg*1 C_{20} C_{30}	169.0 ± 24.4	235 ± 8	−89.7 ± 12.2	2016.08–2024.07
Fingerprint *Deg*1 C_{20} C_{30}	161.2 ± 23.5	241 ± 8	−59.6|−55.5 ± 11.7	
Fingerprint ALT *Deg*1 C_{20} C_{30}	134.3 ± 23.3	238 ± 9	−47.0|−42.7 ± 12.4	2016.08–2023.05
TN-13 *Deg*1 + TN-14 C_{20} C_{30}	117.5 ± 13.5	238 ± 7	−154.7 ± 4.0	2007.01–2016.07
TN-13 *Deg*1 + TN-11E C_{20} C_{30}	98.8 ± 17.8	225 ± 10	−156.2 ± 5.2	
GRACE-OBP *Deg*1 C_{20} C_{30}	110.4 ± 19.6	247 ± 10	−161.2 ± 5.7	
Fingerprint *Deg*1 C_{20} C_{30}	111.9 ± 18.4	259 ± 9	−147.3|−143.2 ± 5.4	
Fingerprint ALT *Deg*1 C_{20} C_{30}	92.4 ± 19.0	267 ± 11	−148.1|−143.9 ± 5.3	
TN-13 *Deg*1 + TN-14 C_{20} C_{30}	187.8 ± 22.4	211 ± 7	−157.6 ± 12.9	2016.08–2022.08
TN-13 *Deg*1 + TN-11E C_{20} C_{30}	144.3 ± 22.2	192 ± 9	−151.8 ± 13.0	
GRACE-OBP *Deg*1 C_{20} C_{30}	205.8 ± 29.3	218 ± 8	−174.2 ± 16.7	
Fingerprint *Deg*1 C_{20} C_{30}	201.8 ± 27.8	221 ± 8	−155.0|−150.9 ± 15.9	
Fingerprint ALT *Deg*1 C_{20} C_{30}	169.4 ± 27.7	222 ± 9	−147.8|−143.2 ± 15.8	

the original GRACE/GRACE-FO coefficients in mass change estimations, making the fingerprint approach a valuable tool for addressing challenges in low-degree coefficient estimation while ensuring compatibility with existing gravity field models.

One key advantage of the fingerprint approach is its forward modeling nature, which directly links gravity field changes to prescribed mass changes. This provides a clear framework for understanding the contributions of various components to each low-degree coefficient, as illustrated by Sun et al. (2019) for C_{20}. Additionally, the fingerprint database offers flexibility by representing global gravity changes, radial crustal displacements, and relative sea level changes, enabling integration with multiple data sources such as gravimetry (GRACE/GRACE-FO), altimetry, GPS, and tide gauges. This versatility enhances its utility for comprehensive Earth system analyses.

Looking ahead, this approach may offer a practical means to mitigate the impact of degraded low-degree coefficients in GRACE/GRACE-FO data, particularly during periods of compromised accelerometer performance. Our current analysis focuses on degree-1, C_{20}, and C_{30}, as we have not identified any additional low-degree coefficients that are significantly affected during the degraded period, nor are we aware of any published reports suggesting otherwise. Nonetheless, the fingerprint framework could, in principle, be extended to additional coefficients if future evidence warrants it. Such an extension would depend on the quality and stability of the higher-degree harmonics used in the fingerprint fitting process, which may themselves be compromised during degraded period. Therefore, even if certain degraded coefficients are not explicitly targeted for recovery through the fingerprint approach, they should be carefully excluded to prevent contamination of the resulting solutions.

In this study, we used the fingerprint database in the form of gravity changes, evaluating results based on GRACE/GRACE-FO data alone and in combination with altimetry data. While incorporating altimetry data generally resulted in smaller annual amplitudes and different linear trends, these outcomes could be improved with better constraints on error information and input data weights. Without this information, the inclusion of altimetry data could introduce additional uncertainties into the results. Another limitation of the fingerprint approach is its

complexity and reliance on a detailed fingerprint database may limit its accessibility and adoption. To address this, we have made the fingerprint database publicly available to facilitate independent low-degree coefficient estimation. However, the method's accuracy is dependent on how well the predefined mass change blocks represent actual spatial characteristics of mass redistribution, which remains imperfectly understood within the Earth system. Future research should aim to refine mass block divisions and improve the representation of mass distribution within each block. Incorporating seismic signals from mega-thrust earthquakes could further reduce residuals in reconstructed fields and improve the accuracy of low-degree coefficient trends. Achieving reliable linear trends, however, remains challenging, as these estimates are influenced by factors such as the choice of GIA model and the inclusion of altimetry data. Continued efforts to enhance the robustness of trend estimates are crucial.

In addition to the above considerations, it is important to acknowledge that our analysis relies on GRACE GSM coefficients, which are derived after removing the AOD1B product that represents atmospheric and oceanic dynamic mass variability. As a result, our findings are implicitly dependent on the accuracy and assumptions of the AOD1B model. Although our fingerprint framework does not explicitly incorporate an OBP model, the use of GSM coefficients assumes that AOD1B effectively removes the high-frequency atmospheric and oceanic signals. It is also worth noting that both atmospheric and oceanic dynamics can, in principle, produce fingerprints contribute to GRACE/GRACE-FO observations. While we do not expect these signals to have a substantial impact on the specific low-degree coefficients examined in this study, a more detailed assessment of their potential influence remains an important direction for future research.

In summary, the fingerprint approach enables the effective simultaneous estimation of multiple low-degree coefficients. These derived coefficients can serve as robust alternatives for completing degree-1 and replacing C_{20} and C_{30}, offering a reliable solution for improving GRACE/GRACE-FO data analyses. By addressing current limitations and pursuing further refinements, this approach has the potential to significantly enhance the accuracy and utility of low-degree coefficients in future gravity field studies.

Data Availability Statement

All data used in this study are publicly available. GRACE/GRACE-FO level-2 data can be accessed on the website of the International Centre for Global Earth Models (ICGEM) (Kvas et al., 2019). Altimeter satellite gridded sea level anomalies are available on the Copernicus Marine Environment Monitoring Service (CMEMS) website (CMEMS, 2023). The Argo data were collected and made freely available by the International Argo Program and the national programs that contribute to it (Argo, 2000). The degree-1 gravity coefficients (TN-13), the CSR SLR C_{20} and C_{30} solutions (TN-11E), and the GFZ SLR C_{20} and C_{30} solutions (TN-14) are available from the website (NASA, 2024). The AIS and GIS drainage basins data are sourced from the Ice sheet Mass Balance Inter-comparison Exercise (IMBIE) website (IMBIE, 2024). The fingerprint databases used in this study are publicly accessible (Mei et al., 2024).

Acknowledgments
We thank the editors and anonymous reviewers for their insightful comments and suggestions, which significantly improved the quality of this work. We also extend our gratitude to Pavel Ditmar from Delft University of Technology for his computation of the uncertainties of our products. This research was supported by the National Natural Science Foundation of China (Grants 42171426, 41801393, and 42304099) and National Key Research and Development Program of China (2025YFE0102700). We estimate AIS mass change time series using a dedicated tool package provided by Feng (2019). All figures were generated using the Generic Mapping Tools (Wessel et al., 2019).

References

Argo. (2000). Argo float data and metadata from Global Data Assembly Centre (Argo GDAC) [Dataset]. *SEANOE*. https://doi.org/10.17882/42182

Bandikova, T., McCullough, C., Kruizinga, G. L., Save, H., & Christophe, B. (2019). GRACE accelerometer data transplant. *Advances in Space Research*, *64*(3), 623–644. https://doi.org/10.1016/j.asr.2019.05.021

Behzadpour, S., Mayer-Gürr, T., & Krauss, S. (2021). GRACE follow-on accelerometer data recovery. *Journal of Geophysical Research: Solid Earth*, *126*(5), e2020JB021297. https://doi.org/10.1029/2020jb021297

Bettadpur, S. (2007). *Level-2 gravity field product user handbook*, *The GRACE Project*. Jet Propulsion Laboratory.

Blewitt, G., Lavallée, D., Clarke, P., & Nurutdinov, K. (2001). A new global mode of Earth deformation: Seasonal cycle detected. *Science*, *294*(5550), 2342–2345. https://doi.org/10.1126/science.1065328

Caron, L., Ivins, E. R., Larour, E., Adhikari, S., Nilsson, J., & Blewitt, G. (2018). GIA model statistics for GRACE hydrology, cryosphere, and ocean science. *Geophysical Research Letters*, *45*(5), 2203–2212. https://doi.org/10.1002/2017GL076644

Chen, J., & Wilson, C. (2008). Low degree gravity changes from GRACE, Earth rotation, geophysical models, and satellite laser ranging. *Journal of Geophysical Research*, *113*(B6), L22607. https://doi.org/10.1029/2007jb005397

Cheng, M., & Ries, J. (2017). The unexpected signal in GRACE estimates of C_{20}. *Journal of Geodesy*, *91*(8), 897–914. https://doi.org/10.1007/s00190-016-0995-5

Cheng, M., & Ries, J. (2023). C_{20} and C_{30} variations from SLR for GRACE/GRACE-FO science applications. *Journal of Geophysical Research: Solid Earth*, *128*(2), e2022JB025459. https://doi.org/10.1029/2022JB025459

CMEMS. (2023). Altimeter satellite gridded Sea Level Anomalies (SLA) data [Dataset]. *Copernicus Marine Environment Monitoring Service*. https://doi.org/10.48670/moi-00148

Coulson, S., Dangendorf, S., Mitrovica, J. X., Tamisiea, M. E., Pan, L., & Sandwell, D. T. (2022). A detection of the sea level fingerprint of Greenland ice sheet melt. *Science*, *377*(6614), 1550–1554. https://doi.org/10.1126/science.abo0926

Dahle, C., Flechtner, F., Murböck, M., Michalak, G., Neumayer, K., Abrykosov, O., et al. (2019). GRACE-FO geopotential gsm coefficients GFZ RL06. *GFZ Data Services*. https://doi.org/10.5880/GFZ.GRACEFO_06_GSM

Ditmar, P. (2018). Conversion of time-varying Stokes coefficients into mass anomalies at the Earth's surface considering the Earth's oblateness. *Journal of Geodesy*, *92*(12), 1401–1412. https://doi.org/10.1007/s00190-018-1128-0

Ditmar, P. (2022). How to quantify the accuracy of mass anomaly time-series based on GRACE data in the absence of knowledge about true signal. *Journal of Geodesy*, *96*(8), 54. https://doi.org/10.1007/s00190-022-01640-x

Duan, X., Guo, J., Shum, C., & Van Der Wal, W. (2009). On the postprocessing removal of correlated errors in GRACE temporal gravity field solutions. *Journal of Geodesy*, *83*(11), 1095–1106. https://doi.org/10.1007/s00190-009-0327-0

Farrell, W. E. (1972). Deformation of the Earth by surface loads. *Reviews of Geophysics*, *10*(3), 761–797. https://doi.org/10.1029/RG010i003p00761

Feng, W. (2019). Gramat: A comprehensive Matlab toolbox for estimating global mass variations from GRACE satellite data. *Earth Science Informatics*, *12*(3), 389–404. https://doi.org/10.1007/s12145-018-0368-0

Gałdyn, F., & Sośnica, K. (2024). Impact of the combination and replacement of SLR-based low-degree gravity field coefficients in GRACE solutions. *Progress in Earth and Planetary Science*, *11*(1), 7. https://doi.org/10.1186/s40645-024-00608-z

Ghobadi-Far, K., Šprlák, M., & Han, S.-C. (2019). Determination of ellipsoidal surface mass change from grace time-variable gravity data. *Geophysical Journal International*, *219*(1), 248–259. https://doi.org/10.1093/gji/ggz292

Han, S.-C., Riva, R., Sauber, J., & Okal, E. (2013). Source parameter inversion for recent great earthquakes from a decade-long observation of global gravity fields. *Journal of Geophysical Research: Solid Earth*, *118*(3), 1240–1267. https://doi.org/10.1002/jgrb.50116

IMBIE. (2024). AIS and GIS drainage basins data [Dataset]. *IMBIE*. Retrieved from http://imbie.org/imbie-3/drainage-basins

Kang, Z., Tapley, B., Chen, J., Ries, J., & Bettadpur, S. (2019). Geocenter motion time series derived from GRACE GPS and LAGEOS observations. *Journal of Geodesy*, *93*(10), 1931–1942. https://doi.org/10.1007/s00190-019-01292-4

Klees, R., Revtova, E., Gunter, B., Ditmar, P., Oudman, E., Winsemius, H., & Savenije, H. (2008). The design of an optimal filter for monthly GRACE gravity models. *Geophysical Journal International*, *175*(2), 417–432. https://doi.org/10.1111/j.1365-246x.2008.03922.x

Kusche, J., Schmidt, R., Petrovic, S., & Rietbroek, R. (2009). Decorrelated GRACE time-variable gravity solutions by GFZ, and their validation using a hydrological model. *Journal of Geodesy*, *83*(10), 903–913. https://doi.org/10.1007/s00190-009-0308-3

Kusche, J., & Schrama, E. J. O. (2005). Surface mass redistribution inversion from global GPS deformation and Gravity Recovery and Climate Experiment (GRACE) gravity data. *Journal of Geophysical Research*, *110*(B9), B09409. https://doi.org/10.1029/2004JB003556

Kvas, A., Mayer-Gürr, T., Krauss, S., Brockmann, J. M., Schubert, T., Schuh, W.-D., et al. (2019). The satellite-only gravity field model GOCO06s. In *EGU General Assembly 2019: EGU 2019*.

Landerer, F. W., Flechtner, F. M., Save, H., Webb, F. H., Bandikova, T., Bertiger, W. I., et al. (2020). Extending the global mass change data record: GRACE Follow-On instrument and science data performance. *Geophysical Research Letters*, *47*(12), e2020GL088306. https://doi.org/10.1029/2020GL088306

Li, J., Chen, J., Li, Z., Wang, S.-Y., & Hu, X. (2017). Ellipsoidal correction in grace surface mass change estimation. *Journal of Geophysical Research: Solid Earth*, *122*(11), 9437–9460. https://doi.org/10.1002/2017jb014033

Loomis, B. D., Rachlin, K. E., Wiese, D. N., Landerer, F. W., & Luthcke, S. B. (2020). Replacing GRACE/GRACE-FO C_{30} with Satellite Laser Ranging: Impacts on Antarctic ice sheet mass change. *Geophysical Research Letters*, *47*(3), e2019GL085488. https://doi.org/10.1029/2019GL085488

Mei, C., Sun, Y., & Li, Y. (2024). Data for low-degree spherical harmonic coefficients for GRACE/GRACE-FO gravity field models from the fingerprint approach [Dataset]. *Figshare*. https://doi.org/10.6084/m9.figshare.27932184.v1

Müller Schmied, H., Cáceres, D., Eisner, S., Flörke, M., Herbert, C., Niemann, C., et al. (2021). The global water resources and use model WaterGAP v2.2d: Model description and evaluation. *Geoscientific Model Development*, *14*(2), 1037–1079. https://doi.org/10.5194/gmd-14-1037-2021

NASA. (2024). GRACE documentation [Dataset]. *NASA*. Retrieved from https://podaac.jpl.nasa.gov/gravity/grace-documentation#TechnicalNotes

National Academies of Sciences, Engineering, and Medicine. (2018). *Thriving on our changing planet: A decadal strategy for Earth observation from space*. The National Academies Press. https://doi.org/10.17226/24938

Otosaka, I. N., Shepherd, A., Ivins, E. R., Schlegel, N.-J., Amory, C., van den Broeke, M., et al. (2022). Mass balance of the Greenland and Antarctic ice sheets from 1992 to 2020. *Earth System Science Data Discussions*, *2022*, 1–33.

Otosaka, I. N., Shepherd, A., Ivins, E. R., Schlegel, N.-J., Amory, C., van den Broeke, M. R., et al. (2023). Mass balance of the Greenland and Antarctic ice sheets from 1992 to 2020. *Earth System Science Data*, *15*(4), 1597–1616. https://doi.org/10.5194/essd-15-1597-2023

Peltier, R. W., Argus, D. F., & Drummond, R. (2018). Comment on "An Assessment of the ICE-6G_C (VM5a) Glacial Isostatic Adjustment Model" by Purcell et al. *Journal of Geophysical Research: Solid Earth*, *123*(2), 2019–2028. https://doi.org/10.1002/2016JB013844

Razeghi, M., Han, S.-C., McClusky, S., & Sauber, J. (2019). A joint analysis of GPS displacement and GRACE geopotential data for simultaneous estimation of geocenter motion and gravitational field. *Journal of Geophysical Research: Solid Earth*, *124*(11), 12241–12263. https://doi.org/10.1029/2019JB018289

Rietbroek, R., Brunnabend, S.-E., Kusche, J., Schröter, J., & Dahle, C. (2016). Revisiting the contemporary sea-level budget on global and regional scales. *Proceedings of the National Academy of Sciences*, *113*(6), 1504–1509. https://doi.org/10.1073/pnas.1519132113

Rietbroek, R., Fritsche, M., Brunnabend, S. E., Daras, I., Kusche, J., Schröter, J., et al. (2012). Global surface mass from a new combination of GRACE, modelled OBP and reprocessed GPS data. *Journal of Geodynamics*, *59–60*, 64–71. https://doi.org/10.1016/j.jog.2011.02.003

Rignot, E., & Mouginot, J. (2012). Ice flow in Greenland for the international polar year 2008–2009. *Geophysical Research Letters*, *39*(11). L11501. https://doi.org/10.1029/2012GL051634

Sasgen, I., Groh, A., & Horwarth, M. (2019). GFZ GravIS RL06 ice-mass change products.

Sasgen, I., Groh, A., & Horwath, M. (2020). COST-G GravIS RL01 ice-mass change products.

Seo, K.-W., Kim, J.-S., Youm, K., Chen, J., & Wilson, C. R. (2021). Secular polar motion observed by GRACE. *Journal of Geodesy*, *95*(4), 40. https://doi.org/10.1007/s00190-021-01476-x

Sośnica, K., Jäggi, A., Thaller, D., Beutler, G., & Dach, R. (2014). Contribution of Starlette, Stella, and AJISAI to the SLR-derived global reference frame. *Journal of Geodesy*, *88*(8), 789–804. https://doi.org/10.1007/s00190-014-0722-z

Sun, Y., Ditmar, P., & Riva, R. (2016). Observed changes in the Earth's dynamic oblateness from GRACE data and geophysical models. *Journal of Geodesy*, *90*(1), 81–89. https://doi.org/10.1007/s00190-015-0852-y

Sun, Y., Ditmar, P., & Riva, R. (2017). Statistically optimal estimation of degree-1 and C_{20} coefficients based on GRACE data and an ocean bottom pressure model. *Geophysical Journal International*, *210*(3), 1305–1322. https://doi.org/10.1093/gji/ggx241

Sun, Y., Li, Y., Guo, X., & Guo, J. (2023). Estimating C_{30} coefficients for GRACE/GRACE-FO time-variable gravity field models using the GRACE-OBP approach. *Journal of Geodesy*, *97*(3), 20. https://doi.org/10.1007/s00190-023-01707-3

Sun, Y., Riva, R., & Ditmar, P. (2016). Optimizing estimates of annual variations and trends in geocenter motion and J_2 from a combination of GRACE data and geophysical models. *Journal of Geophysical Research: Solid Earth*, *121*(11), 8352–8370. https://doi.org/10.1002/2016JB013073

Sun, Y., Riva, R., Ditmar, P., & Rietbroek, R. (2019). Using GRACE to explain variations in the Earth's oblateness. *Geophysical Research Letters*, *46*(1), 158–168. https://doi.org/10.1029/2018GL080607

Sun, Y., & Riva, R. E. M. (2020). A global semi-empirical Glacial Isostatic Adjustment (GIA) model based on Gravity Recovery and Climate Experiment (GRACE) data. *Earth System Dynamics*, *11*(1), 129–137. https://doi.org/10.5194/esd-11-129-2020

Sutterley, T. C., & Velicogna, I. (2019). Improved estimates of geocenter variability from time-variable gravity and ocean model outputs. *Remote Sensing*, *11*(18), 2108. https://doi.org/10.3390/rs11182108

Swenson, S., Chambers, D., & Wahr, J. (2008). Estimating geocenter variations from a combination of GRACE and ocean model output. *Journal of Geophysical Research*, *113*(B8), B08410. https://doi.org/10.1029/2007JB005338

Swenson, S., & Wahr, J. (2006). Post-processing removal of correlated errors in GRACE data. *Geophysical Research Letters*, *33*(8), L08402. https://doi.org/10.1029/2005gl025285

Tamisiea, M. E., Hill, E. M., Ponte, R. M., Davis, J. L., Velicogna, I., & Vinogradova, N. T. (2010). Impact of self-attraction and loading on the annual cycle in sea level. *Journal of Geophysical Research*, *115*(C7), C07004. https://doi.org/10.1029/2009JC005687

Tapley, B. D., Bettadpur, S., Watkins, M. M., & Reigber, C. (2004). The Gravity Recovery and Climate Experiment: Mission overview and early results. *Geophysical Research Letters*, *31*(9), L09607. https://doi.org/10.1029/2004GL019920

Tapley, B. D., Watkins, M. M., Flechtner, F., Reigber, C., Bettadpur, S., Rodell, M., et al. (2019). Contributions of GRACE to understanding climate change. *Nature Climate Change*, *9*(5), 358–369. https://doi.org/10.1038/s41558-019-0456-2

Wessel, P., Luis, J. F., Uieda, L., Scharroo, R., Wobbe, F., Smith, W. H. F., & Tian, D. (2019). The Generic Mapping Tools version 6. *Geochemistry, Geophysics, Geosystems*, *20*(11), 5556–5564. https://doi.org/10.1029/2019GC008515

Wiese, D., & Yuan, D.-N. (2024). *Tellus level-4 Antarctica mass anomaly time series from JPL GRACE/GRACE-FO Mascon CRI Filtered Release 06.3 version 04*, *NASA Physical Oceanography Distributed Active Archive Center (DAAC) Data Set*. TEMSC.

Wu, X., Heflin, M. B., Ivins, E. R., & Fukumori, I. (2006). Seasonal and interannual global surface mass variations from multisatellite geodetic data. *Journal of Geophysical Research*, *111*(B9), B09401. https://doi.org/10.1029/2005JB004100

Zajdel, R., Sośnica, K., Dach, R., Bury, G., Prange, L., & Jäggi, A. (2019). Network effects and handling of the geocenter motion in multi-GNSS processing. *Journal of Geophysical Research: Solid Earth*, *124*(6), 5970–5989. https://doi.org/10.1029/2019JB017443

Zwally, H. J., Giovinetto, M. B., Li, J., Cornejo, H. G., Beckley, M. A., Brenner, A. C., et al. (2005). Mass changes of the Greenland and Antarctic ice sheets and shelves and contributions to sea-level rise: 1992–2002. *Journal of Glaciology*, *51*(175), 509–527. https://doi.org/10.3189/172756505781829007

References From the Supporting Information

Ditmar, P., Teixeira da Encarnação, J., & Hashemi Farahani, H. (2012). Understanding data noise in gravity field recovery on the basis of inter-satellite ranging measurements acquired by the satellite gravimetry mission GRACE. *Journal of Geodesy*, *86*(6), 441–465. https://doi.org/10.1007/s00190-011-0531-6

Dobslaw, H., Bergmann-Wolf, I., Dill, R., Forootan, E., Klemann, V., Kusche, J., & Sasgen, I. (2015). The updated ESA Earth System Model for future gravity mission simulation studies. *Journal of Geodesy*, *89*(5), 505–513. https://doi.org/10.1007/s00190-014-0787-8

Dobslaw, H., Bergmann-Wolf, I., Forootan, E., Dahle, C., Mayer-Gürr, T., Kusche, J., & Flechtner, F. (2016). Modeling of present-day atmosphere and ocean non-tidal de-aliasing errors for future gravity mission simulations. *Journal of Geodesy*, *90*(5), 423–436. https://doi.org/10.1007/s00190-015-0884-3

Gruber, T., Bamber, J. L., Bierkens, M. F. P., Dobslaw, H., Murböck, M., Thomas, M., et al. (2011). Simulation of the time-variable gravity field by means of coupled geophysical models. *Earth System Science Data*, *3*(1), 19–35. https://doi.org/10.5194/essd-3-19-2011

Kusche, J., & Klees, R. (2002). Regularization of gravity field estimation from satellite gravity gradients. *Journal of Geodesy*, *76*(6–7), 359–368. https://doi.org/10.1007/s00190-002-0257-6